Dynamics of Structure Formation and Crystallization in Asymmetric Diblock Copolymers

Daniel J. Quiram[†] and Richard A. Register*

Department of Chemical Engineering, Princeton University, Princeton, New Jersey 08544

Gary R. Marchand[‡]

The Dow Chemical Company, P.O. Box 400, Plaquemine, Louisiana 70765

Anthony J. Ryan[§]

Manchester Materials Science Centre, University of Manchester Institute of Science and Technology, Manchester M1 7HS, United Kingdom

Received June 5, 1997; Revised Manuscript Received September 23, 1997[⊗]

ABSTRACT: The crystallization behavior of a series of ethylene-*b*-(3-methyl-1-butene) diblocks (E/MB) is investigated via simultaneous, time-resolved small-angle and wide-angle X-ray scattering. All the diblocks contain 26−27 wt % E, but possess varying molecular weights and hence varying segregation strengths in the melt, ranging from homogeneous to strongly segregated. Crystallization from homogeneous or weakly segregated melts at typical rates yields a semicrystalline solid consisting of alternating E and MB lamellae. By contrast, a strongly segregated diblock shows crystallization within the E cylinders that are present in the melt, even for slow crystallization rates and at temperatures where both blocks are well above their glass transition temperatures. Modest differences in intercylinder spacing between the melt at high temperatures and solid at low temperatures are shown to arise from the temperature dependence of the intercylinder spacing in the melt. Because chain diffusion in these block copolymer melts is not always fast on the crystallization time scale, the value of the melt spacing that is "frozen in" upon crystallization depends on the specimen's thermal history. Despite the marked differences in the final structure between polymers where crystallization is constrained to cylinders and those where it "breaks out" to form lamellar microdomains, the kinetics are not remarkably different, at least in these polyethylene-based systems.

I. Introduction

Microphase separation in semicrystalline block copolymers can be driven either by block incompatibility or by crystallization of one or more blocks. We recently examined[1] the interaction between these two phenomena in a series of ethylene-*b*-(3-methyl-1-butene) (E/MB) diblocks of constant composition (26−27 wt % E) and varying molecular weight. Through small-angle X-ray scattering experiments on the highest molecular weight (88 kg/mol) material, we demonstrated that strong segregation could confine crystallization to preestablished cylindrical microdomains, even when both blocks are well above their glass transitions at the crystallization temperature and the crystallization rate is slow. When the melt is weakly segregated (M_w = 44 kg/mol), the crystalline morphology and domain spacing were found to be strong functions of thermal history; the E crystals were not necessarily confined to the E cylinders formed in the melt. Here, we dynamically probe the microphase separation and crystallization processes in this series of E/MB diblock copolymers through simultaneous synchrotron-based small-angle (SAXS) and wide-angle X-ray scattering (WAXS).

Several time-resolved studies have investigated the crystallization of diblock copolymers from both homogeneous[2,3] and weakly segregated melts.[3−5] In the two studies involving crystallization of ethylene-based diblock copolymers from single-phase melts,[2,3] both groups concluded that E block crystallization and microdomain formation follow the same growth kinetics. The lamellar domain period and size distribution were found to be invariant during microstructure development, suggesting that the ordered structures nucleate and grow to fill the sample, with no concurrent internal rearrangement. As expected for crystalline materials that form a spherulitic superstructure, the crystallization kinetics were well represented by the Avrami equation.

The presence of an ordered melt mesophase in block copolymers presents an added complexity to the crystallization process.[1,3−12] Previous time-resolved studies have involved block copolymers with weakly segregated melts, revealing that crystallization destroys any preexisting melt microstructure in forming a lamellar morphology.[3−5] (Throughout this paper, "lamellar" refers to the microdomain structure, that is, alternating layers of E and MB. This should be distinguished from the E crystallites, which may also be lamellar but which occur on a smaller length scale *within* the E lamellae or cylinders.) Rangarajan *et al.*[4] examined the crystallization of an ethylene-*b*-(head-to-head propylene) copolymer (E/hhP) from a weakly segregated lamellar melt (order−disorder transition temperature $T_{ODT} \approx 125$ °C) and found that crystallization induced rearrangement into a lamellar morphology of larger domain spacing at the expense of the previous structure. The final morphology of the E/hhP diblock was found to be path-dependent (sensitive to minor changes in thermal history) due to melt segregation. Ryan *et al.*[3] examined the crystallization of a series of ethylene-*b*-ethylethylene (E/EE) copolymers of varying E block composition from microphase-separated melts. Of particular relevance to

* To whom correspondence should be addressed.
† Present address:The Procter & Gamble Company, Winton Hill Technical Center, Cincinnati, OH 45244.
‡ Present address:Dow-DuPont Elastomers L.L.C., P.O. Box 400, Plaquemine, LA 70765-0400.
§ Present address:Department of Chemistry, University of Sheffield, Brookhill, Sheffield S3 7HF, U.K.
⊗ Abstract published in *Advance ACS Abstracts,* December 1, 1997.

S0024-9297(97)00805-X CCC: $14.00

Table 1. Characterization Data

sample	M_w (kg/mol)	f_E	T_{ODT} (°C)	E T_m (°C)	E T_c 10 °C/min (°C)	E T_c 20 °C/min (°C)
E/MB35	34.7	0.26	<110	107	80	74
E/MB44	44.3	0.26	167	105	71	62
E/MB63	62.7	0.27	>260	105	62	60
E/MB88	87.9	0.27	>260	103	62	61
dE19	19.0	1	N/A	111	95	

the present work is a material with an f_E (weight fraction E block) of 0.25 ($T_{ODT} \approx 255$ °C), which formed a morphology of E cylinders packed onto a hexagonal lattice in an EE matrix in the melt. Upon crystallization, destruction of the cylindrical melt morphology was accompanied by transformation into a lamellar structure with a larger domain spacing. The crystallization process was well modeled with the Avrami equation in both cases.[3,4] Nojima *et al.*[5] probed crystallization in a series of ϵ-caprolactone-*b*-butadiene (CL/B) copolymers of varying CL block composition through time-resolved SAXS. Despite the different polymer chemistry, crystallization of the CL block again destroyed any microphase-separated structure present, increasing the domain spacing of the crystallized sample relative to the melt. Thus, for moderate degrees of melt segregation where both blocks are fluid ($T > T_g$), crystallization disrupts the melt mesophase to form a lamellar crystalline morphology.

This study tracks the crystallization dynamics in materials of varying block incompatibility in the melt. Special emphasis is placed on the process where crystallization is confined to hexagonally packed cylinders. These results are compared with weakly segregated melts displaying crystallization-induced conversion of the melt microstructure into a lamellar morphology.

II. Experimental Section

A. Synthesis and Molecular Characterization. The E/MB precursors (high-1,4-butadiene)-*b*-(high-3,4-isoprene) were synthesized via sequential anionic polymerization in cyclohexane; detailed descriptions of the synthesis and molecular characterization are given elsewhere.[1,3] To create the high-3,4 isoprene precursor to the MB block, 1,2-dipiperidinoethane (DPE) was added at a concentration of 2 mol/mol of Li initiator after polymerization of the 1,4-butadiene block.[14] The E/MB diblocks were prepared from the precursors by exhaustive hydrogenation at 100 °C and 400 psi in heptane using unreduced palladium on barium sulfate as the catalyst.[15] Fourier transform infrared spectroscopy (FTIR) was used to verify that there was no residual unsaturation in the samples. High-temperature gel-permeation chromatography of the E/MB diblocks at 135 °C in 1,2,4-trichlorobenzene showed that no backbone changes occurred as a result of hydrogenation. The ODT temperatures of the materials were determined via SAXS as described in Adams *et al.*[16] A summary of the characterization information is presented in Table 1, where the diblocks are labeled as E/MB followed by the overall molecular weight (in kilograms per mole). Deuterated E19 (dE19) is a fully saturated polybutadiene homopolymer (saturated with D_2 gas; $M_w = 19.0$ kg/mol, neglecting additional mass of deuterium over hydrogen) of similar microstructure to the E block in the E/MB copolymers; the hydrogenated analogue has been characterized previously.[17,18] Final melting temperatures (T_m) at 10 °C/min and peak crystallization temperatures (T_c) were determined using a Perkin-Elmer DSC-7 calibrated with indium and mercury.

B. Time-Resolved Experiments. Time-resolved simultaneous SAXS/WAXS experiments were conducted at beamline 8.2 of the Synchrotron Radiation Source in Daresbury, U.K.,[2−4,19] using a beam of $\lambda = 0.154$ nm X-rays measuring 3×0.3 mm^2 at the sample position. A 0.5−0.9 mm thick film of polymer sample was enclosed in a cell made of standard aluminum differential scanning calorimetry (DSC) pans (TA Instruments) with holes punched in both the pan and the lid and covered with 20 μm thick mica windows. These pans were placed in a modified Linkam THM microscope hot stage interfaced with a high-resolution dc temperature controller. A 1.0×2.5 mm^2 slot in the heater block and cell holder allowed X-rays access to the sample.[20] Scattering from the empty cell (including the DSC pan and windows) was subtracted from all SAXS data. Cooling of the sample cell was achieved via cold nitrogen vapor pumped through the heater block. Steady-state values of the cell temperature were verified by comparison of crystallization half-times ($t_{1/2}$) with those obtained from isothermal crystallization on these samples conducted on a Perkin-Elmer DSC-7.[13] The SAXS data were collected with a Daresbury quadrant detector for which angular calibration was achieved using a wet rat tail tendon ($d = 67.0$ nm) and a lamellar styrene-*b*-(1,4-isoprene)-*b*-styrene copolymer ($d = 28.0$ nm), which has been characterized previously.[21] The SAXS data presented here were subsequently smoothed with a series of triangle functions, two five-point triangles or a five-point and a three-point triangle being used for $q < 0.2$ nm^{-1}. Here, the scattering vector $q = (4\pi/\lambda) \sin \theta$, where θ is half the scattering angle. The WAXS data were acquired with a curved INEL detector that was calibrated with a high-density polyethylene standard. Subsequent smoothing of the WAXS data employed a three-point triangle function for the crystalline reflections and additional triangle functions for the data outside the crystalline peaks. The areas under the crystallite reflections (I_c) and the amorphous hump (I_a) in the WAXS data can be used to estimate the weight fraction crystallinity (w_c) within the E block:

$$w_c = \frac{1}{f_E}\left(\frac{I_c}{I_c + I_a}\right) \tag{1}$$

Data from the simultaneous SAXS/WAXS isothermal crystallization runs are compiled in Table 2, including the initial (at T_c, following crystallization) and final (at 30 °C, after cooling from T_c at 50 °C/min) values for w_c and the primary peak position, q^*. These data will be discussed in Section III. Due to the greater uncertainty for $q < 0.14$ nm^{-1} (± 0.008 nm^{-1} vs ± 0.003 nm^{-1} for $q > 0.14$ nm^{-1}), q values below 0.14 nm^{-1} are displayed to two significant figures. The w_c values obtained from the WAXS data by eq 1 were systematically high vs DSC, because the low-2θ part of the amorphous hump falls outside the experimental angular range, leading to an underestimate of I_a. Consequently, a correlation was developed between the WAXS w_c values at 30 °C and the DSC w_c values presented in ref 1. The w_c values given in Table 2 are from the correlation and are therefore on an absolute scale (based on DSC values).

Prior to the first SAXS/WAXS run, each sample was compression-molded at 140 °C into a 0.5−0.9 mm thick film which was cooled to room temperature at roughly 50 °C/min. The temperature profile for the time-resolved experiments was as follows. Run 1: 1 min hold at 30 °C, followed by a 20 °C/min ramp up to the melt temperature (T_{melt}, see Table 2), 1 min hold at T_{melt}, followed by 50 °C/min cooldown to the crystallization temperature (T_c, see Table 2). Subsequent Runs: 1 min hold at 30 °C, followed by a 50 °C/min ramp up to T_{melt}, 1 min hold at T_{melt}, followed by 50 °C/min cool-down to the crystallization temperature (T_c). Data acquisition commenced after the 1 min hold at 30 °C; each SAXS or WAXS frame consists of the intensity integrated over 6 s.

III. Results and Discussion

A. Crystallization from Strongly Segregated Melts. Two samples in this E/MB series form strongly segregated ($T_{ODT} > 260$ °C), hexagonally packed cylindrical melts: E/MB63 and E/MB88. Previously, we showed conclusive evidence that crystallization is confined to the cylindrical microdomains in E/MB88 when the material is cooled from the melt at 10−20 °C/min.[1] Due to the relatively large domain spacing of E/MB88 [(10) interplanar spacing $d_{10} = 51$ nm], the primary peak

Table 2. Isothermal Crystallization Results

sample	T_c (°C)	T_{melt} (°C)	q^* at T_c (nm^{-1})	q^* at 30 °C (nm^{-1})	w_c at T_c	w_c at 30 °C	$t_{1/2}$ second peak/shoulder (s)	n second peak
E/MB35	quench	140		0.215		0.34		
E/MB35	93	144	0.13	0.14	0.16	0.34	305	2.0
E/MB35	89	144	0.13	0.141	0.22	0.34	147	3.0
E/MB35	85	144	0.13		0.32		84	3.2
E/MB44	quench	140		0.206		0.33		
E/MB44	88	185	0.12	0.13	0.29	0.33	750	2.6
E/MB44	86	185	0.13	0.13	0.28	0.34	394	3.6
E/MB44	82	185	0.143	0.143	0.29	0.34	212	4.0
E/MB44	80	185	0.149	0.152	0.29	0.34	128	3.7
E/MB63	quench	140		0.148		0.29		
E/MB63	80	142	0.12	0.13	0.24	0.31	406	2.5
E/MB63	77	142	0.13	0.12	0.24	0.31	271	2.9
E/MB63	73	142	0.13	0.13	0.25	0.31	182	3.4
E/MB63	69	142	0.12		0.24		89	3.3
E/MB88	quench	140	*a*	*a*		0.26		
E/MB88	74	143	*a*	*a*	0.24	0.30	446	2.1
E/MB88	69	143	*a*	*a*	0.22	0.30	194	1.8
E/MB88	67	143	*a*	*a*	0.26		114	1.7
dE19	quench	140		0.49		0.31		
dE19	101	146	0.20		0.13		211	3.2

[a] Primary peak obstructed by beam stop.

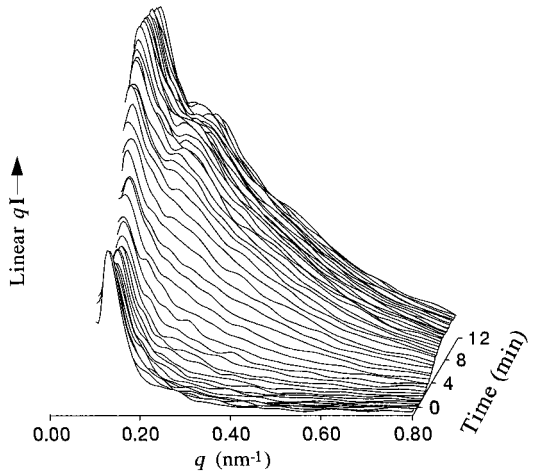

Figure 1. Time-resolved SAXS data for E/MB63 during crystallization at 77 °C following cooling from a 142 °C melt at 50 °C/min. For clarity, every three data sets have been averaged so that each curve represents the intensity integrated over an 18 s period. The point at which the hot stage first reaches 77 °C is set as zero time.

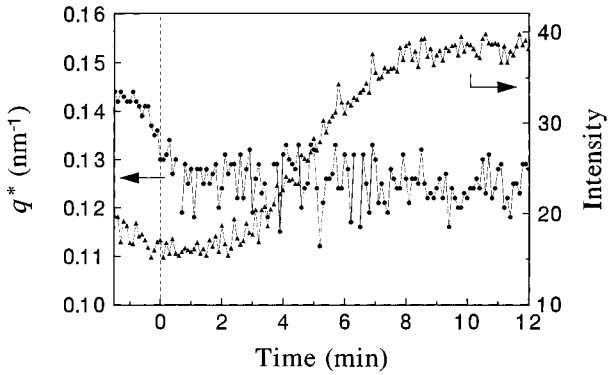

Figure 2. Primary peak position (q^*, ●) and intensity (▲) plotted as functions of time for the data shown in Figure 1. The point at which the hot stage first reaches 77 °C is set as zero time. Intensity is in arbitrary units. A substantial decrease in q^* is observed prior to crystallization.

was obstructed by the beamstop during the time-resolved experiments. Despite having a 28% lower molecular weight, E/MB63 also exhibits cylindrically confined crystallization independent of thermal history, as shown by the retention of hexagonal symmetry in the two-dimensional SAXS pattern of an oriented specimen.[13]

Time-resolved SAXS data (q-corrected) detailing the crystallization of E/MB63 are shown in Figure 1. During this experiment, the sample was cooled at 50 °C/min from 142 °C down to 77 °C, where the subsequent crystallization was monitored. In the melt at 142 °C, a narrow, intense primary peak indicative of microphase separation is evident with $q^* = 0.144$ nm^{-1} ($d_{10} = 43.6$ nm). Both q^* and the intensity of the primary peak for the profiles in Figure 1 are plotted as functions of time in Figure 2. Zero time corresponds to the point at which the thermocouple first registers 77 °C. The intensity increase of the primary SAXS peak beginning near 3 min is due to crystallization of the E block, as discussed in more detail below. Prior to crystallization, q^* decreases from its value in the 142 °C melt, corresponding to a 10% increase in the intercylinder spacing. However, within 1 min after reaching the crystallization temperature, and throughout the crystallization process, q^* is constant to within the experimental uncertainty. This trend in the melt results from a combination of changes in density, statistical segment length, and block incompatibility with temperature; a change of similar magnitude was previously observed in a styrene-*b*-(ethylene-*alt*-propylene) melt by Sakurai *et al.*[22] Thus, differences in the Bragg spacing between the 142 °C melt and the crystalline material at 77 °C result from the temperature dependence of the intercylinder spacing in the melt rather than from any rearrangement induced by crystallization.

Equilibration of the domain spacing in the melt following a temperature change necessarily requires chain diffusion. This requirement is most obvious for a spherical morphology, where an increase in the sphere size mandates the assimilation of additional blocks of the sphere-former; nonetheless, the same is true for lamellar and cylindrical morphologies as well. The situation is most easily visualized by considering a single "grain", where the cylindrical or lamellar director is uniform, and requiring that the overall dimensions of the grain be constant while the microdomain spacing

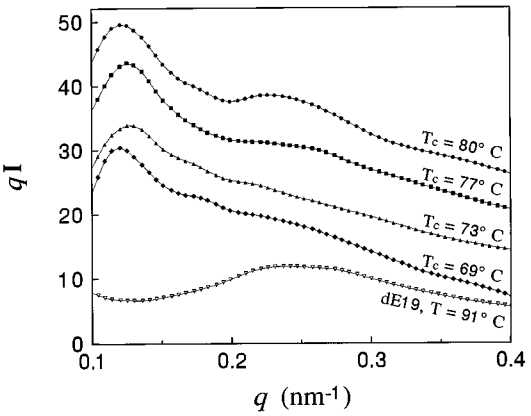

Figure 3. SAXS profiles taken on semicrystalline E/MB63 and dE19 at varying crystallization temperatures. The E/MB63 profiles were taken after long times ($t > 2t_{1/2}$); thus, each sample had achieved the fullest possible crystallization at the given temperature. The dE19 profile was taken at 91 °C during melting and has been scaled to account for the relative amount of E block in E/MB63. The profiles have been shifted along the intensity axis (arbitrary units) for clarity. Note the differences in the E/MB63 profiles around $q = 0.23$ nm^{-1}.

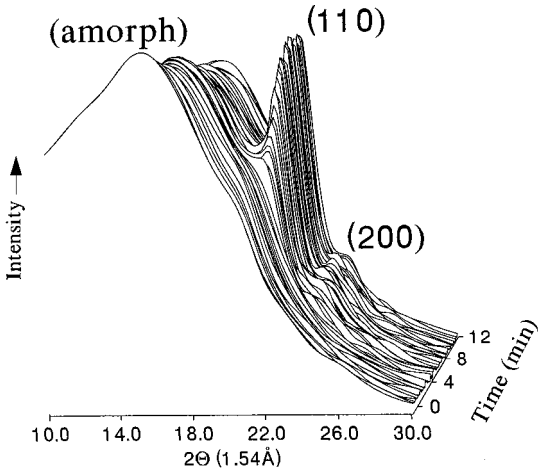

Figure 4. Time-resolved WAXS data for E/MB63 crystallizing at 77 °C, corresponding to the SAXS data shown in Figure 1. For clarity, every three data sets have been averaged so that each curve represents the intensity integrated over an 18 s period. The point at which the hot stage first reaches 77 °C is set as zero time.

changes. (The alternative, a change in the grain structure induced by temperature, would require chain diffusion on even larger length scales, approaching those of the grain.) For E/MB63, Figure 2 shows that the domain spacing (as gauged by q^*) continues to change for about 1 min after the sample has reached the crystallization temperature. For deeper quenches, significant crystallization can occur within 1 min, indicating that the time required for the Bragg spacing in the melt to equilibrate is not always fast on the time scale of interest. For example, Table 2 shows that the quenched E/MB63 sample exhibits its primary peak at $q^* = 0.148$ nm^{-1}, indicating that the cylinders present in the melt had not fully equilibrated prior to the onset of crystallization.

On cooling to 30 °C, q^* retains the value it had at T_c to within experimental error (see Table 2), though the crystallinity increases significantly. While crystallization might be expected to reduce d_{10} through densification, and thus increase q^*, based on temperature-dependent densities of E and MB[23−26] and the w_c values in Table 2, less than a 1% decrease in q^* is expected upon crystallization at 77 °C. The values of w_c at both T_c and 30 °C are independent of T_c; values of w_c measured by DSC for E/MB63 crystallized at various temperatures[13] show this same independence from T_c.

The SAXS data in Figure 1 also exhibit a pronounced shoulder on the high-q side of the primary peak. While it may initially appear that this is a higher order peak from the E/MB microdomain structure (*e.g.*, at $\sqrt{3}$ for hexagonally packed cylinders), the position of this feature actually varies with the crystallization temperature. SAXS patterns at four different crystallization temperatures ($t > 2t_{1/2}$) are plotted in Figure 3 (upper four curves). These profiles are composed of scattering from two different sources: first, a relatively narrow structure factor peak due to the (10) distance between semicrystalline cylinders, and second, a broad, intense peak due to scattering from the crystallites formed inside the cylinders. For the first source, to within the experimental uncertainty, q^* is invariant with crystallization temperature. The second source should resemble the scattering observed in saturated polybutadiene homopolymers (such as dE19) or in E-containing diblocks that crystallize from single-phase or weakly segregated melts; the crystal thicknesses are essentially identical in all those cases[3] because the thickness is controlled by the number of ethyl branches (saturated 1,2-butadiene units) in the E block. However, note that the crystallites in E/MB63 are confined to cylindrical microdomains, whereas in E homopolymers or block copolymers where crystallization controls the microdomain structure,[27] they form lamellae of large lateral extent. For comparison, the bottom profile in Figure 3 shows dE19 data at 91 °C, exhibiting a broad peak centered near $q = 0.24$ nm^{-1}. The E/MB63 sample crystallized at 80 °C displays a high-q peak at 0.23 nm^{-1}, that crystallized at 77 °C displays a shoulder in the same vicinity, while those crystallized at 73 and 69 °C do not even exhibit a clear shoulder. This trend is consistent with a broadening of the SAXS peak in hydrogenated polybutadiene and a shift to higher q as the crystallization temperature is reduced.[21] Thus, despite confinement to cylinders and the obvious constraint on their lateral extent, the crystallites in E/MB63 show scattering resembling that from E homopolymers.

Figure 4 shows the WAXS data taken in the same run as the SAXS data of Figure 1. In the melt, an intense, broad peak due to scattering from amorphous material is observed. This peak decreases in intensity (and area) as the (110) and (200) reflections of the orthorhombic PE crystal[25,27] begin to grow. As described in Section IIB, the WAXS profiles allow for calculation of w_c, values of which (at T_c and 30 °C) are displayed in Table 2. As judged by Figures 1 and 4, the crystalline reflections appear to develop on the same time scale as the increase in SAXS primary peak intensity. To investigate this further, it is useful to replot the data in the Avrami form, which is commonly used to analyze crystallization processes:

$$\ln(1 - X_c) = -kt^n \tag{2}$$

Here, X_c is the fraction of crystallization process that has occurred at elapsed time t, n is the Avrami exponent, and k is a constant related to the nucleation density and growth rate. We obtain X_c from

$$X_c = \frac{I(t) - I_0}{I_m - I_0} \tag{3}$$

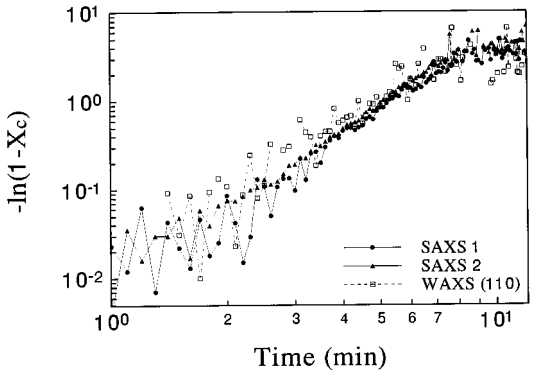

Figure 5. Avrami plot of the crystallization of E/MB63 at 77 °C (data taken from Figures 1 and 4). Crystallization results based on the intensity of the primary SAXS peak (●), secondary SAXS shoulder (▲), and (110) WAXS reflection (□) are plotted, and all three data sets show the same time course.

where I_0 is the melt scattering intensity at T_c (determined from data sets immediately after t_0), I_m is the intensity at the end of the experiment, and $I(t)$ represents the intensity at time t. If the SAXS and WAXS intensities truly develop in parallel, then their Avrami plots will superimpose regardless of whether the data actually follow the Avrami model—that is, whether or not they show a constant, integral value of n.

An Avrami plot for E/MB63 crystallized at 77 °C is shown in Figure 5, based on the intensities of the primary SAXS peak (SAXS 1), the shoulder (SAXS 2), and the WAXS (110) reflections. The SAXS and WAXS reflections grow concurrently, indicating that E crystallization is driving the intensity increase observed by SAXS. Table 2 lists values of $t_{1/2}$ and n obtained from the intensity increase of the second peak/shoulder; for E/MB88, though the primary peak was obscured by the beamstop, the higher-q shoulder was clearly visible and allowed $t_{1/2}$ and n values to be determined. Since crystallization is confined to cylinders, making spherulite formation impossible,[1,13] it is surprising to see that the Avrami exponents for E/MB63 and E/MB88 vary from 1.7 to 3.4, values commonly observed for polymers that crystallize in spherulites. Thus, the peculiar crystallization behavior of E/MB63 is not reflected in the value of n.

B. Crystallization from Weakly Segregated and Homogeneous Melts. A lower molecular weight sample, E/MB44, exhibits a weakly segregated melt with T_{ODT} = 167 °C. Time-resolved SAXS data taken on cooling E/MB44 from 185 to 82 °C at 50 °C/min and monitoring the subsequent crystallization are shown in Figure 6. At 185 °C, a correlation hole peak[28] is evident at $q^* = 0.22$ nm^{-1}. Upon decreasing the temperature below T_{ODT}, an increase in intensity and decrease in peak width can be observed resulting from microphase separation. The peak intensity begins to increase at 160 °C and does not reach its maximum until 115 °C, due to the finite rate of microphase separation coupled with a few degree lag between the sample and thermocouple temperatures during scanning. Approximately 3 min after reaching 82 °C, the peak present in the melt begins to decrease in intensity and is replaced by a new set of three peaks corresponding to the crystallized polymer. The simultaneous growth of three distinct peaks (q ratio of 1:2:3) indicates that crystallization results in the development of a lamellar morphology at the expense of the cylindrical melt morphology.

Both q^* (of the melt and crystalline peaks) and intensity (of the primary crystalline peak) are plotted as functions of time in Figure 7. At approximately 3.5 min, the peak from the lamellar solid becomes evident, and by 4 min the scattering from the crystallized fraction has so overwhelmed that from the molten fraction that the original melt peak is no longer evident. When the Avrami equation is applied to the E/MB44 SAXS and WAXS data, a good overlap between the two is observed, indicating that crystallization drives the formation of the final lamellar morphology. Avrami exponents listed in Table 2 range from 2.6 to 4.0 as expected for spherulitic crystallization, but again, these values are not dissimilar to those found for E/MB63 where crystallization occurs within cylinders. These results serve as a caveat: with only a limited range of times over which the Avrami plots appear linear (less than a full decade in our case), inferences about the structure based on the Avrami exponent are dubious at best.

Table 2 shows that, for E/MB44, q^* decreases with increasing T_c, with only minor increases on cooling from

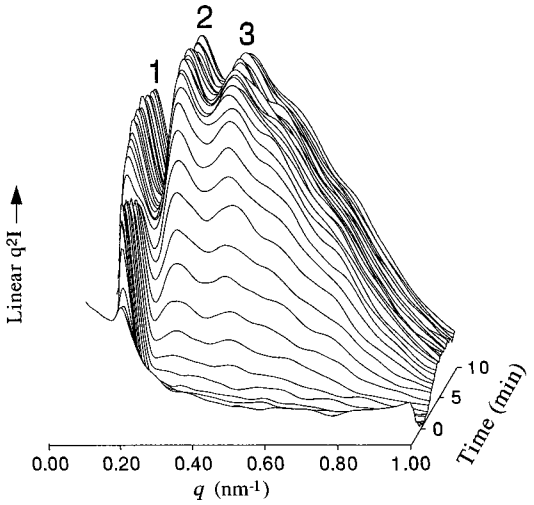

Figure 6. Time-resolved SAXS data for E/MB44 during crystallization at 82 °C following cooling from a 185 °C melt at 50 °C/min. For clarity, every three data sets have been averaged so that each curve represents the intensity integrated over an 18 s period. The point at which the hot stage first reaches 82 °C is set as zero time; 2 min of melt data are shown in the figure prior to t = 0. The reflection orders in the crystallized sample are labeled (1, 2, 3); the intensity of the first-order peak is less than that of the two higher-order peaks due to a superposition of scattering from the lamellar E-MB microstructure plus scattering from the crystallites within the E domains.[3,4,27]

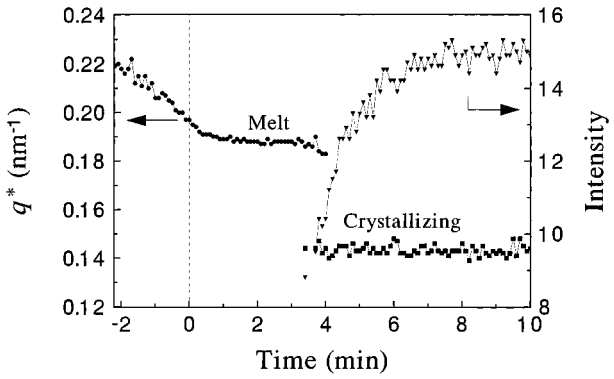

Figure 7. Positions (q^*) of the primary peaks corresponding to the cylindrical melt (●) and lamellar solid (■) as functions of time for the data of Figure 6. Also shown is the intensity of the first-order peak for the lamellar solid (▼). The point at which the hot stage first reaches 82 °C is set as zero time.

T_c to 30 °C. The strong dependence of Bragg spacing on T_c is consistent with prior results from our group regarding the crystallization of a symmetric E/hhP from a weakly segregated melt.[4] A decrease in q^* of approximately 30% is evident in the isothermally crystallized samples vs the quenched sample, as expected since quenching kinetically constrains crystallization to the cylindrical microdomains.[1] E/MB35, which crystallizes from a homogeneous melt, also exhibits a lamellar crystalline morphology. Though the domain spacing is essentially identical for the samples crystallized isothermally at 85−93 °C, q^* is quite different for the quenched sample (crystallized on cooling at 50 °C/min). Previous studies[2,27] on ethylene-*b*-(ethylene-*alt*-propylene) diblocks crystallizing from homogeneous melts showed no such dependence of domain spacing on crystallization conditions; the differing results for E/MB35 are most likely due to the proximity of the ODT in E/MB35 to the crystallization temperature.

IV. Conclusions

Time-resolved SAXS/WAXS on a series of crystallizable E/MB diblocks (26−27 wt % E, varying molecular weight) shows that the strength of melt segregation can have a profound effect on the solid-state structure. Furthermore, in a given diblock, the rate of crystallization significantly affects the periodicity observed in the final semicrystalline solid. In a diblock crystallizing from a homogeneous melt (E/MB35) close to its ODT, despite the polymer's compositional asymmetry, a solid-state structure consisting of alternating E and MB lamellae is always formed. The spacing observed in the solid depends on the crystallization rate, as the proximity of this diblock to its ODT retards the chain diffusion necessary to form the final structure. In a weakly segregated diblock (E/MB44, T_{ODT} = 167 °C), crystallization at typical rates eradicates the melt morphology (E cylinders in an MB matrix) and produces a lamellar structure, where again the microdomain spacing in the crystallized solid (corresponding to the overall E-MB periodicity) can be adjusted by changing the crystallization rate. By contrast, rapid quenching (50 °C/min) of this same diblock results in a qualitatively different structure: crystallization is restricted to the E cylinders that are present in the melt.

In the case of a strongly segregated diblock (E/MB63), crystallization occurs within the E cylinders for any crystallization history. This demonstrates that strongly-segregated melts can effectively template crystallization even when both blocks are well above their glass transition temperatures. Modest changes in intercylinder spacing between the melt at high temperatures and the solid at low temperatures are due to the temperature dependence of the intercylinder spacing in the melt, rather than to destruction of the cylinders on crystallization. Provided that crystallization is slow enough that the intercylinder spacing can equilibrate before significant crystallization occurs, the structure in the final solid is independent of the crystallization rate. However, if the material is quenched rapidly, the melt structure does not fully equilibrate prior to the onset of crystallization, and a different periodicity is observed in the final product. The E crystallites within the cylinders in E/MB63 contribute a feature to the small-angle scattering pattern resembling that from hydrogenated polybutadiene homopolymers, despite the obvious constraint on the lateral extent of the crystallites imposed by the cylinders. Though crystallization within cylinders precludes the formation of spherulites, the kinetics of crystallization as monitored by SAXS/WAXS are not markedly different from those of homogeneous or weakly segregated crystallizable diblocks that do form spherulites. This points out the difficulty in making a direct connection between the observed kinetics and the mode of crystal growth.

Acknowledgment. This work was supported by the National Science Foundation, through the Polymers Program (DMR-9257565), while travel to Daresbury Laboratory was supported through the NATO Collaborative Research Grants Program (CRG 951243). We gratefully acknowledge the EPSRC for beamtime at Daresbury and thank Dr. Pratima Rangarajan and Dr. J. Patrick A. Fairclough for their experimental assistance.

References and Notes

(1) Quiram, D. J.; Register, R. A.; Marchand, G. R. *Macromolecules* **1997**, *30*, 4551.
(2) Rangarajan, P.; Register, R. A.; Adamson, D. H.; Fetters, L. J.; Bras, W.; Naylor, S.; Ryan, A. J. *Macromolecules* **1995**, *28*, 1422.
(3) Ryan, A. J.; Hamley, I. W.; Bras, W.; Bates, F. S. *Macromolecules* **1995**, *28*, 3860.
(4) Rangarajan, P.; Register, R. A.; Fetters, L. J.; Bras, W.; Naylor, S.; Ryan, A. J. *Macromolecules* **1995**, *28*, 4932.
(5) Nojima, S.; Kato, K.; Yamamoto, S.; Ashida, T. *Macromolecules* **1992**, *25*, 2237.
(6) Cohen, R. E.; Cheng, P. L.; Douzinas, K.; Kofinas, P.; Berney, C. V. *Macromolecules* **1990**, *23*, 324.
(7) Khandpur, A. K.; Macosko, C. W.; Bates, F. S. *J. Polym. Sci., B: Polym. Phys.* **1995**, *33*, 247.
(8) Sakurai, K.; MacKnight, W. J.; Lohse, D. J.; Schulz, D. N.; Sissano, J. A. *Macromolecules* **1993**, *26*, 3236.
(9) Tepe, T.; Schulz, M. F.; Zhao, J.; Tirrell, M.; Bates, F. S.; Mortensen, K.; Almdal, K. *Macromolecules* **1995**, *28*, 3008.
(10) Schnablegger, H.; Rein, D. H.; Rempp, P.; Cohen, R. E. *J. Polym. Eng.* **1996**, *16*, 1.
(11) Robitaille, C.; Prud'homme, J. *Macromolecules* **1983**, *16*, 665.
(12) Séguéla, R.; Prud'homme, J. *Polymer* **1989**, *30*, 1446.
(13) Quiram, D. J. Ph.D. Thesis, Princeton University, Princeton, NJ, 1997.
(14) Mays, J.; Hadjichristidis, N.; Fetters, L. J. *Macromolecules* **1984**, *17*, 2723.
(15) Rosedale, J. H.; Bates, F. S. *J. Am. Chem. Soc.* **1988**, *110*, 3542.
(16) Adams, J. L.; Quiram, D. J.; Graessley, W. W.; Register, R. A.; Marchand, G. R. *Macromolecules* **1996**, *29*, 2929.
(17) Rangarajan, P.; Haisch, C. F.; Register, R. A.; Adamson, D. H.; Fetters, L. J. *Macromolecules* **1997**, *30*, 494.
(18) Ueda, M. M.S.E. Thesis, Princeton University, Princeton, NJ, 1995.
(19) Bras, W.; Derbyshire, G. E.; Ryan, A. J.; Mant, G. R.; Felton, A.; Lewis, R. A.; Hall, C. J.; Greaves, G. N. *Nucl. Instrum. Methods Phys. Res., Sect. A* **1993**, *326*, 587.
(20) Bras, W.; Derbyshire, G. E.; Devine, A.; Clark, S. M.; Cooke, J.; Komanschek, B. E.; Ryan, A. J. *J. Appl. Crystallogr.* **1995**, *28*, 26.
(21) Rangarajan, P. Ph.D. Thesis, Princeton University, Princeton, NJ, 1995.
(22) Sakurai, S.; Hashimoto, T.; Fetters, L. J. *Macromolecules* **1995**, *28*, 7947.
(23) Krishnamoorti, R. Ph.D. Thesis, Princeton University, Princeton, NJ, 1994.
(24) Graessley, W. W.; Krishnamoorti, R.; Reichart, G. C.; Balsara, N. P.; Fetters, L. J.; Lohse, D. J. *Macromolecules* **1995**, *28*, 1260.
(25) Howard, P. R.; Crist, B. *J. Polym. Sci., B: Polym. Phys.* **1989**, *27*, 2269.
(26) Brandrup, J.; Immergut, E. H., Eds. *Polymer Handbook*, 3rd ed.; Wiley: New York, 1989.
(27) Rangarajan, P.; Register, R. A.; Fetters, L. J. *Macromolecules* **1993**, *26*, 4640.
(28) Leibler, L. *Macromolecules* **1980**, *13*, 1602.

MA9708050